Supporting Information

Cu-based electrode material for controlled selective electrooxidation of tetrahydroisoquinoline

Yizhou Zhang,[a] Rongxian Zhang,*[a] Qi Zhang,[a] Yilin Deng,[b] Jiexin Guan,[b] Yizhou Ling,[c] and Guoxing Zhu*[a]

[a] Chemistry and Chemical Engineering, Jiangsu University, Zhenjiang, 202013, China.

[b] Institute for Energy Research, Jiangsu University, Zhenjiang, 202013, China.

[c] School of Education Science, Nanjing Normal University, Nanjing 210097, China.

* Corresponding authors: rong@ujs.edu.cn; zhuguoxing@ujs.edu.cn.

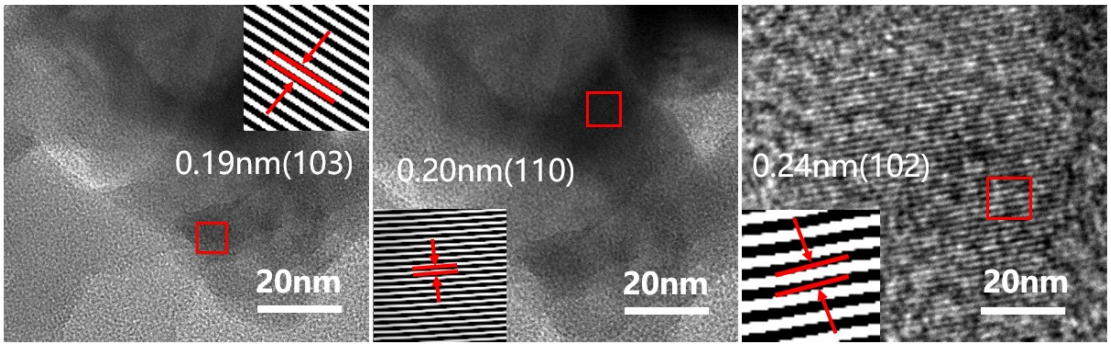

Fig. S1 TEM images of the Cu_2S/NF.

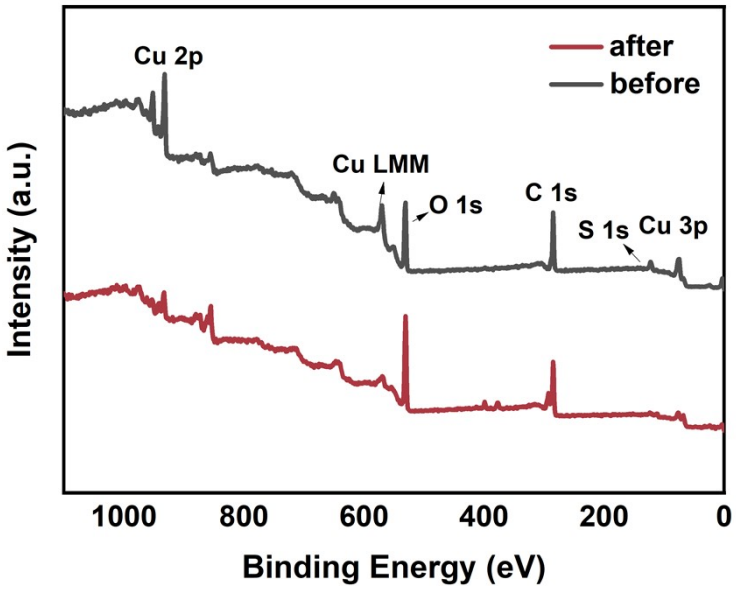

Fig. S2 XPS spectra of the Cu_2S catalytic electrode before and after catalysis.

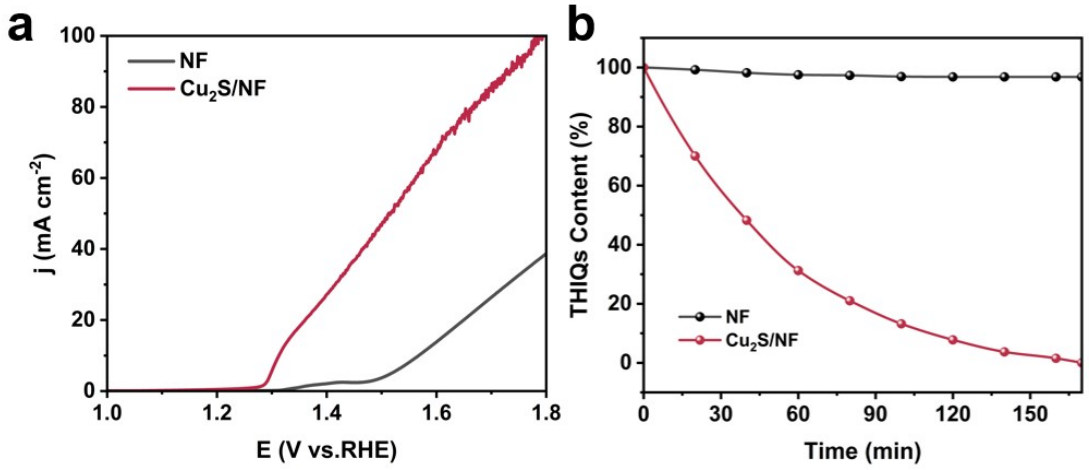

Fig. S3 (a) LSV comparison curves of NF and Cu_2S/NF; (b) Comparison curves of THIQ content between NF and Cu_2S/NF.

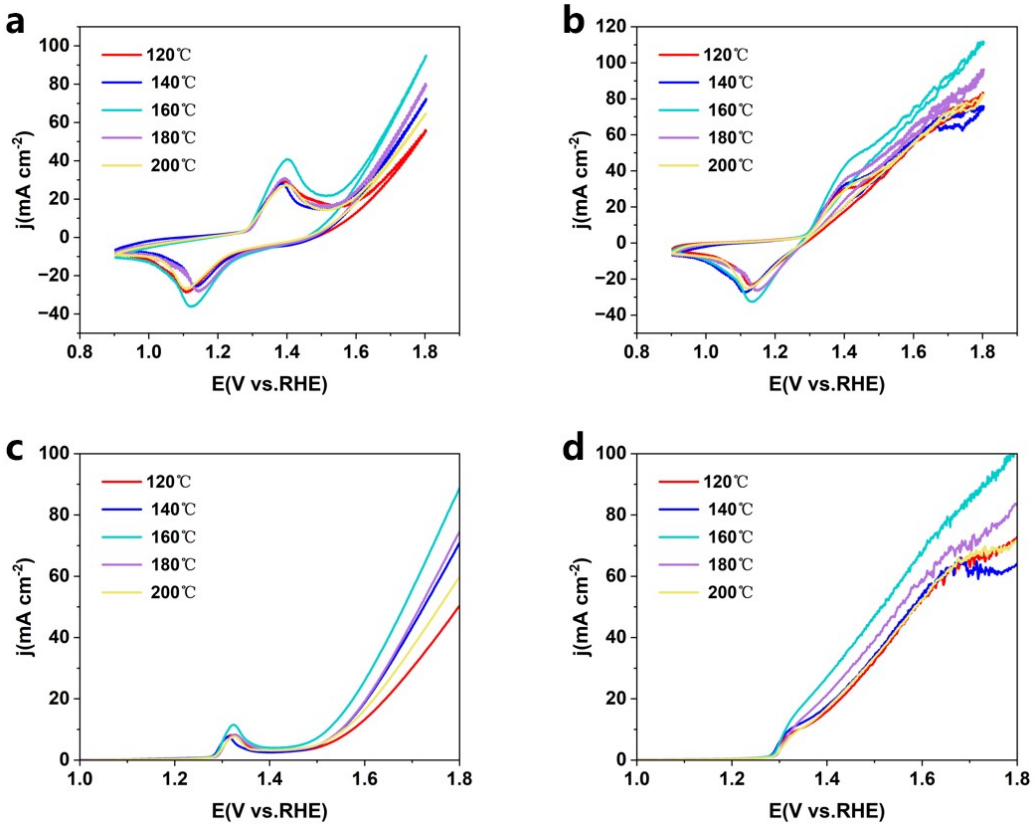

Fig. S4 Performance of Cu_2S prepared at different hydrothermal temperatures. (a) CV curves without THIQs; (b) CV curves with THIQs; (c) LSV curves without THIQs; (d) LSV curves with THIQs.

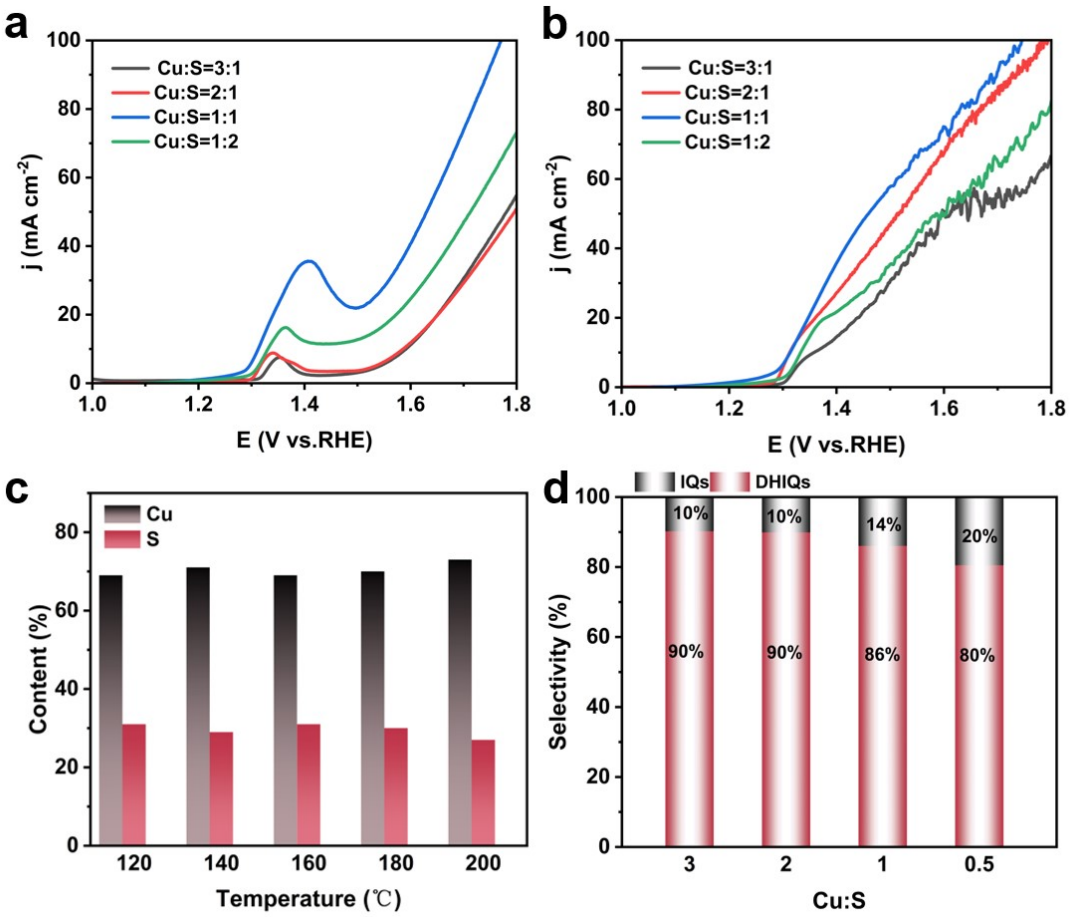

Fig. S5 Catalytic activity of the electrodes with different Cu/S ratios. (a) LSV curves without THIQ, (b) LSV curves with THIQ. (c) Cu/S ratios of the electrodes obtained at different preparation temperatures. (d) catalytic selectivity.

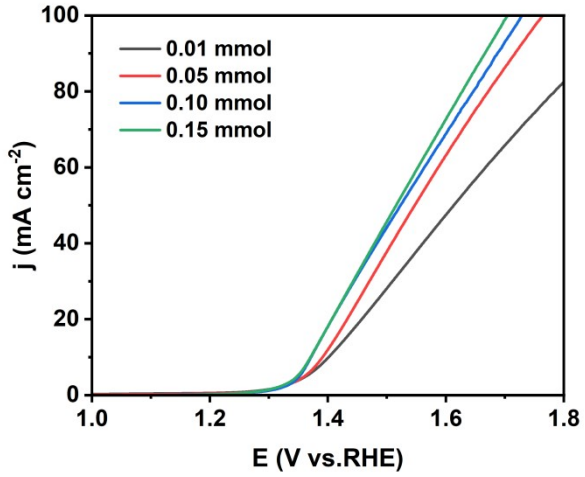

Fig. S6 LSV curves obtained in 1.0 M KOH with different dosages of THIQs.

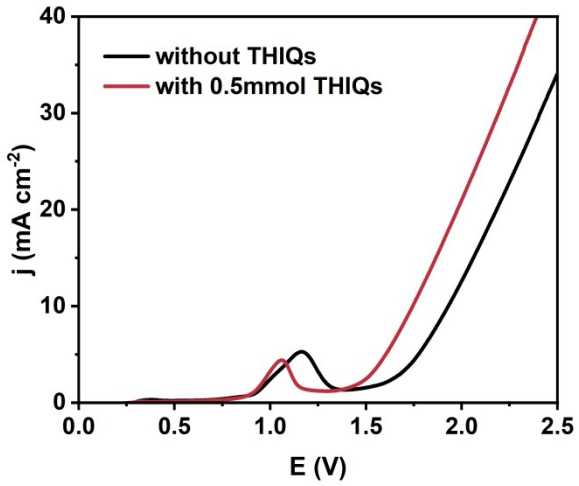

Fig. S7 LSV curves over the Cu_2S/NF||Cu_2S/NF electrolyzed in the presence or absence of THIQs.

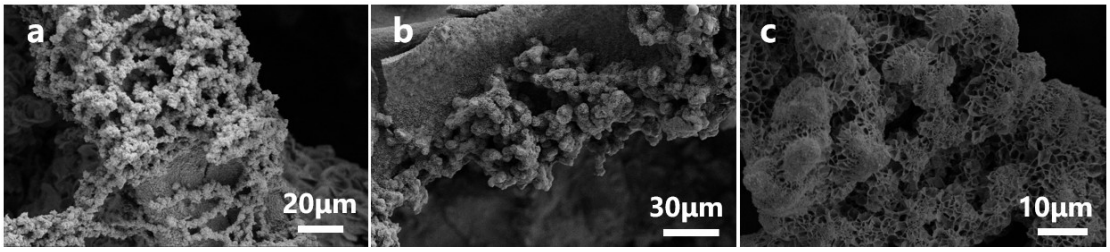

Fig. S8 SEM images of Cu_2S/NF (a) before the reaction; (b) and (c) after the reaction.

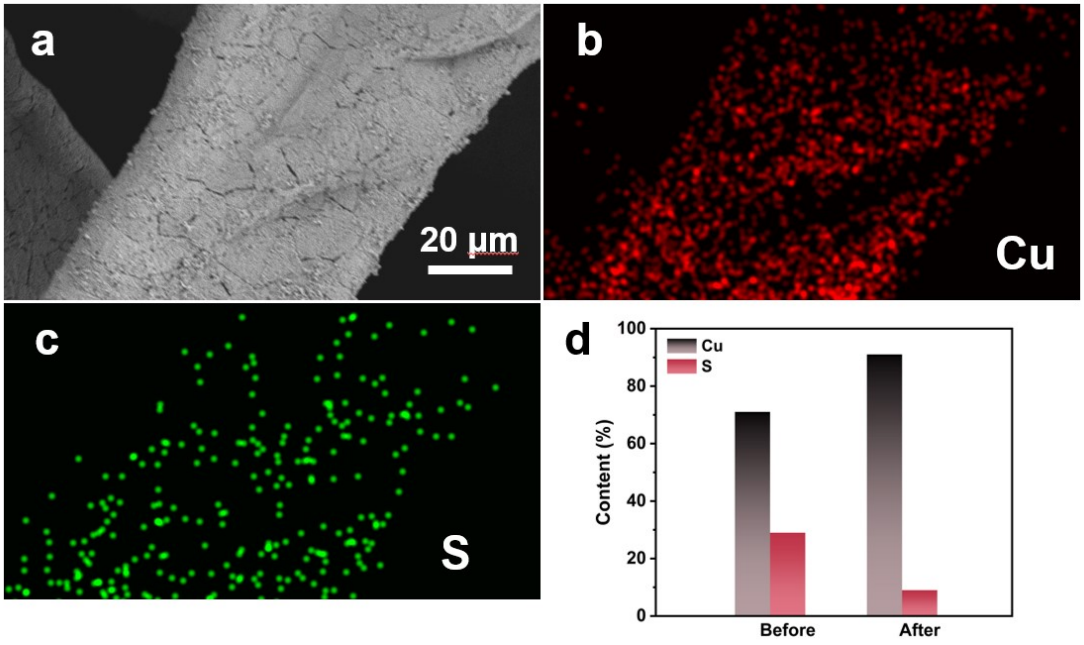

Fig. S9 (a-c) EDS images of Cu_2S/NF. (d) Cu/S ratios before and after the reaction.

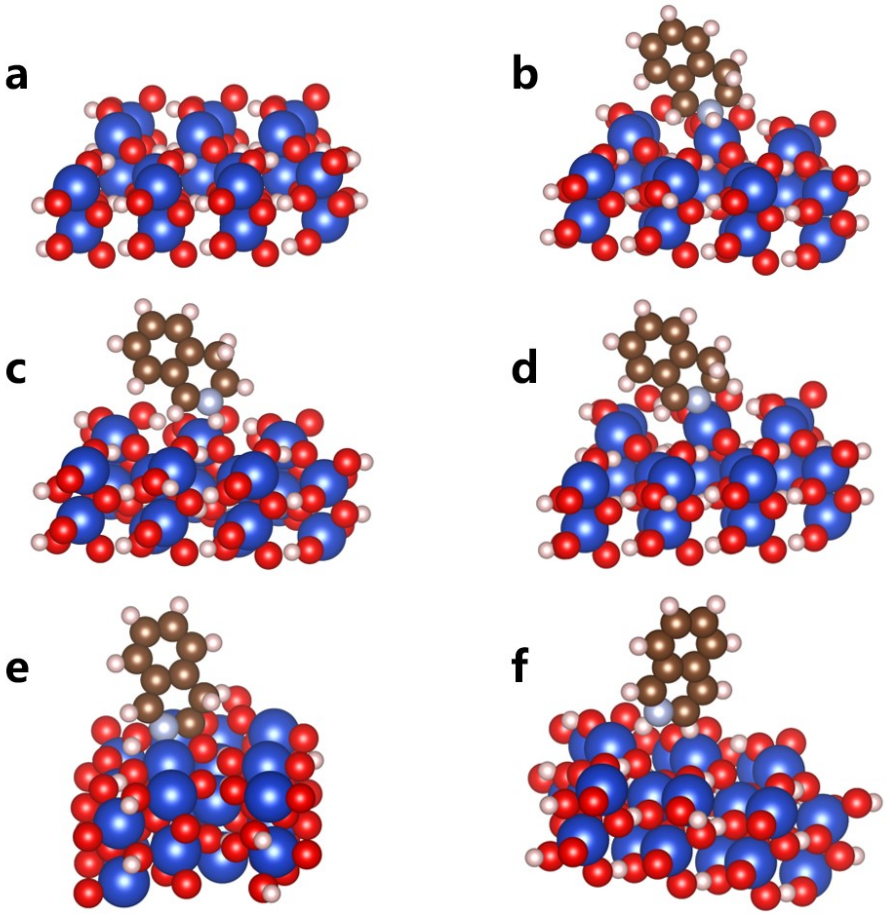

Fig. S10 Space-filling models for (a) CuOOH; (b) CuOOH-THIQ; (c) CuOOH-$THIQ_{ads}$; (d) CuOOH-DHIQ; (e) CuOOH-$DHIQ_{ads}$; (f) CuOOH-IQ.

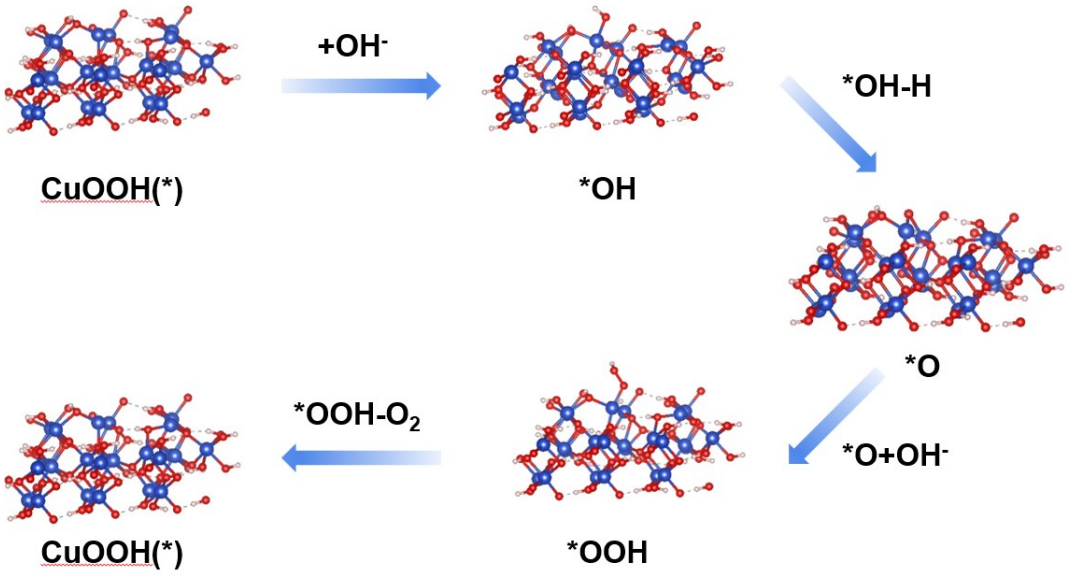

Fig. S11 OER steps on CuOOH.

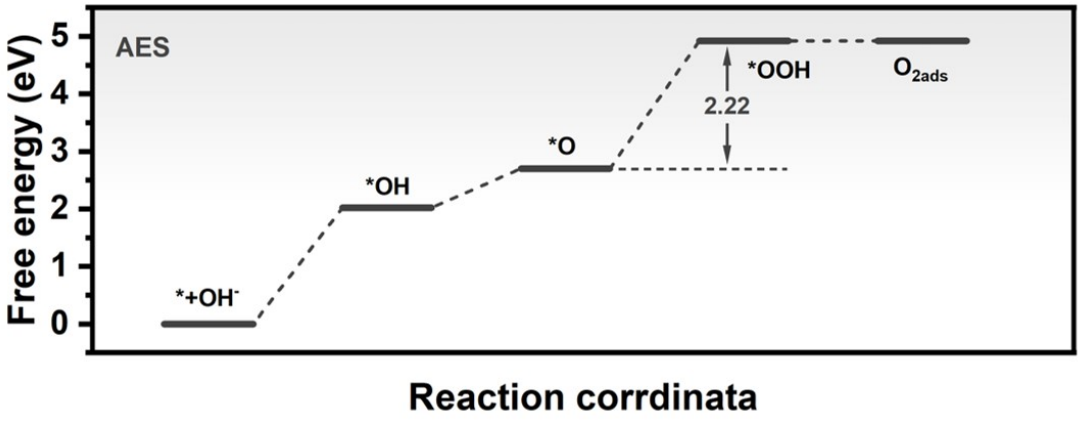

Fig. S12 Gibbs free energy of the AES reaction path of oxygen evolution reactions.

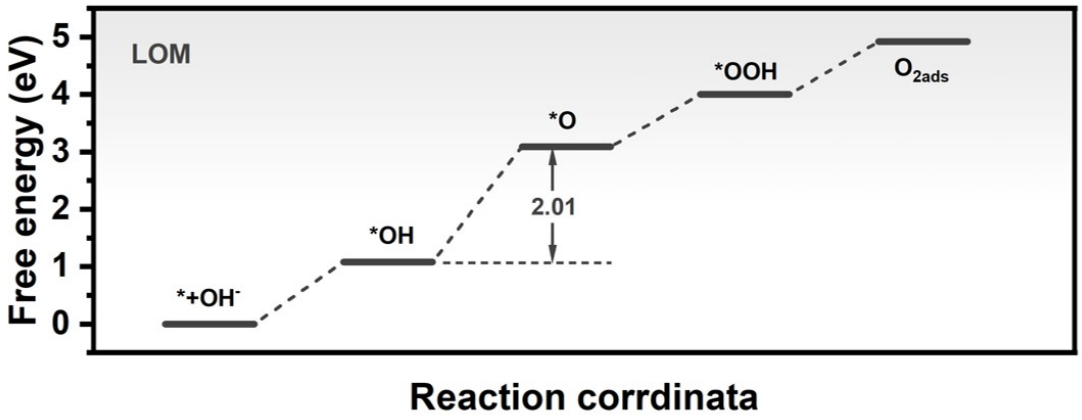

Fig. S13 Gibbs free energy of the LOM reaction path of oxygen evolution reactions.

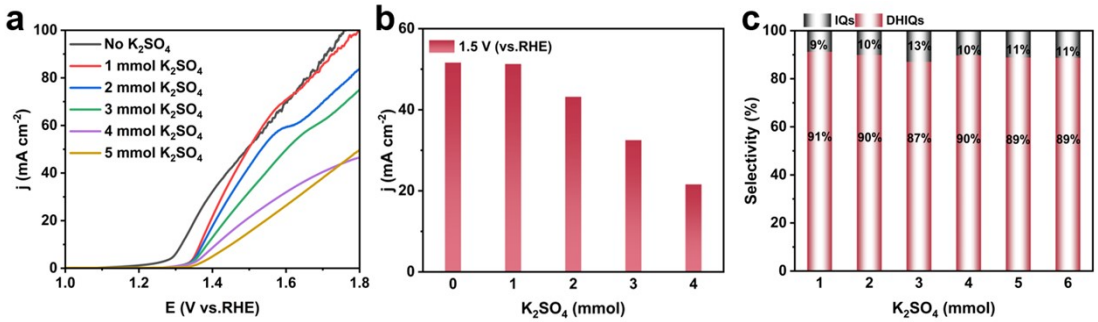

Fig. S14 (a) LSV curves at different K_2SO_4 contents; (b) difference in current density at different K_2SO_4 contents; (c) Selectivity at different K_2SO_4 contents.

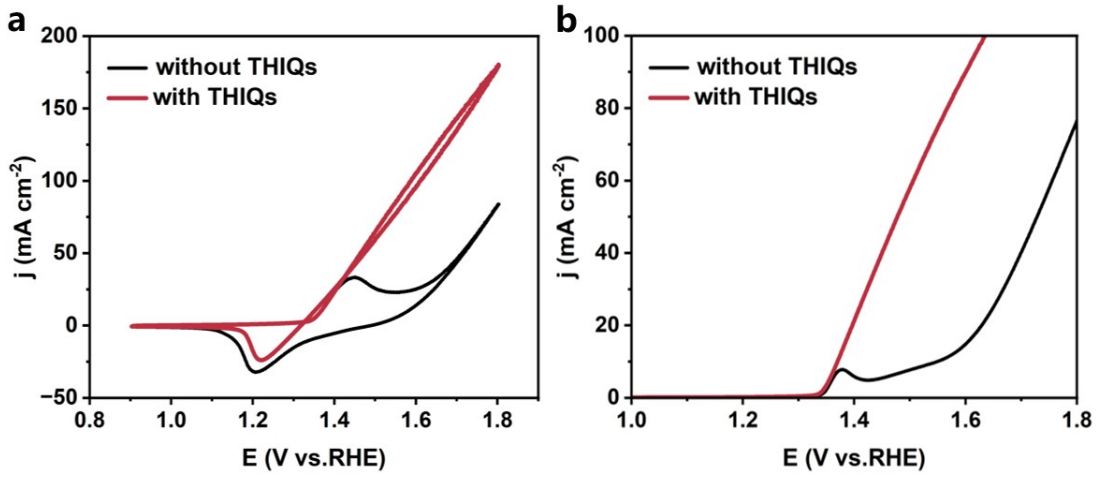

Fig. S15 (a) CV and (b) LSV curves collected on the Cu_2S anode with 1.0 M KOH in the presence or absence of Urea.

Tab. S1 Performance comparison of the dehydrogenation reaction.

Catalysts	Catalytic types	Reaction time	Reaction temperature	Conversion	Yield [%]		Refs.
					DHIQs	IQs	
MOF-253-$Ru(dcbpy)_2$	photocatalysis	5 days	room temperature	91.1	78.3	8.0	1
DMF	thermocatalysis	24 h	100 °C	>95	84	/	2
$MoS_2/ZnIn_2S_4$	photocatalysis	12 h	room temperature	94	85	9	3
TiO_2	photocatalysis	24 h	room temperature	100	93	/	4
Ni_2P	electrocatalysis	1 h	room temperature	>99	99	/	5
Ni-NSA-V_{Ni}	electrocatalysis	/	room temperature	98	98	0	6
Co_3O_4@NF	electrocatalysis	1 h	room temperature	81	72	/	7
Ni_3N	electrocatalysis	1 h	room temperature	100	79	21	8
NiMo-P	electrocatalysis	1 h	room temperature	100	80.2	19.8	9
Cu_2S	electrocatalysis	2.8 h	room temperature	100	90	10	This work

Tab. S2 Gibbs free energy of the reaction steps.

Step	ΔG/eV
CuOOH+THIQ→*THIQ	-1.37
THIQ-H→$THIQ_{ads}$	0.01
*THIQ-H→*DHIQ	0.39
DHIQ-H→$DHIQ_{ads}$	-1.18
*$DHIQ_{ads}$-H→*IQ	2.46

*: adsorption; ads: Intermediate state.

References

1 X. Deng, Y. Qin, M. Hao and Z. Li, MOF-253-Supported Ru Complex for Photocatalytic CO_2 Reduction by Coupling with Semidehydrogenation of 1,2,3,4-Tetrahydroisoquinoline (THIQ), *Inorg. Chem.*, 2019, **58**, 16574-16580.

2 A. Mollar-Cuni, D. Ventura-Espinosa, S. Martín, H. García and J. A. Mata, Reduced Graphene Oxides as Carbocatalysts in Acceptorless Dehydrogenation of N-Heterocycles, *ACS Catal*, 2021, **11**, 14688-14693.

3 M. Hao, X. Deng, L. Xu and Z. Li, Noble metal Free $MoS_2/ZnIn_2S_4$ nanocomposite for acceptorless photocatalytic semi-dehydrogenation of 1,2,3,4-tetrahydroisoquinoline to produce 3,4-dihydroisoquinoline, *Appl Catal B-Environ*, 2019, **252**, 18-23.

4 N. O. Balayeva, N. Zheng, R. Dillert and D. W. Bahnemann, Visible-Light-Mediated Photocatalytic Aerobic Dehydrogenation of N-heterocycles by Surface-Grafted TiO_2 and 4-amino-TEMPO, *ACS Catal*, 2019, **9**, 10694-10704.

5 C. Huang, Y. Huang, C. Liu, Y. Yu and B. Zhang, Integrating Hydrogen Production with Aqueous Selective Semi-Dehydrogenation of Tetrahydroisoquinolines over a Ni_2P Bifunctional Electrode, *Angew Chem Int Ed*, 2019, **58**, 12014-12017.

6 C. Wang, W. Zhou, Z. Sun, Y. Wang, B. Zhang and Y. Yu, Integrated selective nitrite reduction to ammonia with tetrahydroisoquinoline semi-dehydrogenation over a vacancy-rich Ni bifunctional electrode, *J Mater Chem A*, 2021, **9**, 239-243.

7 M. Xiang, Z. Xu, J. Wang, X. Yang and Z. Yan, Accelerating H_2 Evolution by Anodic

Semi-dehydrogenation of Tetrahydroisoquinolines in Water over Co_3O_4 Nanoribbon Arrays Decorated Nickel Foam, 2021, **27**, 7502-7506.

8 R. Zhang, N. Chen, T. Ning, Y. Zhang, Y. Ling, X. Wang, W. Zhu and G. Zhu, Branched Porous Ni_3N as a Catalytic Electrode for Selective Semidehydrogenation of Tetrahydroisoquinoline, *Inorg. Chem.*, 2023, **62**, 17433-17443.

9 N. Chen, R. Zhang, W. Sun, Y. Zhang, S. Li, Q. Zhang, H. Yang, Y. Deng, Y. Ling and G. Zhu, Surface Reconstruction for Selective Oxidation of Tetrahydroisoquinoline, *Inorg. Chem.*, 2024, **63**, 8977-8987.